

PCCP

Accepted Manuscript



This is an *Accepted Manuscript*, which has been through the Royal Society of Chemistry peer review process and has been accepted for publication.

Accepted Manuscripts are published online shortly after acceptance, before technical editing, formatting and proof reading. Using this free service, authors can make their results available to the community, in citable form, before we publish the edited article. We will replace this *Accepted Manuscript* with the edited and formatted *Advance Article* as soon as it is available.

You can find more information about *Accepted Manuscripts* in the [Information for Authors](#).

Please note that technical editing may introduce minor changes to the text and/or graphics, which may alter content. The journal's standard [Terms & Conditions](#) and the [Ethical guidelines](#) still apply. In no event shall the Royal Society of Chemistry be held responsible for any errors or omissions in this *Accepted Manuscript* or any consequences arising from the use of any information it contains.



Cite this: DOI: 10.1039/xxxxxxxxxx

Viscometry of single nanoliter-volume droplets using dynamic force spectroscopy[†]

Manhee Lee,^{a‡} Bongsu Kim,^a QHwan Kim,^a JongGeun Hwang,^a Sangmin An,^a and Wonho Jhe^{*a}

Received Date
Accepted Date

DOI: 10.1039/xxxxxxxxxx

www.rsc.org/journalname

The viscometry of minute amounts of liquids has been on high demand as a novel tool for medical diagnosis and biological assays. Various microrheological techniques have shown the capability to handle small volumes. However, as the liquid volume decreases down to nanoliter scale, the increasingly dominant surface effects complicate the measurement and analysis, which remains a challenge in microrheology. Here, we demonstrate an atomic force microscope-based platform that determines the viscosity of single sessile drops of 1 nanoliter Newtonian fluids. We circumvent the interfacial effects by measuring the negative-valued shear elasticity, originating from the retarded fluidic response inside the drop. Our measurement is independent of the liquid-boundary effects, and thus valid without a priori knowledge of surface tension or contact angle, which consistently holds at 1 milliliter-scale volume. Importantly, whereas the previous methods typically need much larger 'unrecoverable' volume above 1 microliter, our simple scheme uses only ~1 nanoliter. Our results offer quantitative and unambiguous methodology of viscosity measurement for extremely minute Newtonian liquids at nanoliter scale.

Introduction

Viscosity is one of fundamental characteristics of fluids that often needs to be measured in diverse physical, chemical and biomedical experiments. In particular, the viscosity measurement of fluids in a human body has been studied for medical diagnosis tools, showing that a wide range of maladies can be predicted by measuring simply the viscosity of the biological fluids^{1–4}. Nonetheless, due to the painful extraction from patients and numerous refining processes involved, the use of minimal amounts of sample has been on increasing demand, which has triggered development of microrheometers such as microfluidic^{5–9} and micro-electro-mechanical system (MEMS)^{10,11} viscometers in addition to the popular particle-tracking technique^{12–15}.

In essence, these methods probe the fluidic response of the bulk phase inside the finite liquid volume. Consequently, as the volume decreases, there inevitably arises the interfacial boundary effects, which complicate accurate measurements and limit the minimal measurable volume. For example, the particle-tracking microrheology detects the motions of the particles suspended in a fluid, from which one can extract the fluidic properties such

as viscosity. In this method, the minimum sample volume is approximately 1 microliter or higher to ensure the particles are free of hydrodynamic interactions with the sample boundaries^{12,14}. For the microfluidic chip, one can derive the viscosity at a steady shear rate by measuring the flow rate of liquids under constant pressure. While the microfluidic technique demonstrated recently the viscosity measurement using 30 nanoliter volume⁷, sizable effects of interfacial tension and associated capillary pressure limit the lower measurable volume. The MEMS replicates the conventional rheometers, which dynamically shear an entire fluid body confined between two plates and measure the fluid response. Although this miniaturized rheometer has reduced the sample volume down to 5 nanoliter¹⁰, the measured quantities are highly sensitive to surface rheology due to the air-liquid surface deformation involved during shear, and thus demands a fine model to extract the viscosity from the measured quantities. In addition, the liquid-immersed resonators have been used to measure the viscosity of the medium fluids at microliter scale^{16–18}, needed to enclose the resonator systems and avoid the hydrodynamic interaction with boundary surfaces.

Here, we present an atomic force microscope (AFM)-based platform that determines the viscosity of single sessile drops of Newtonian fluid at 1 nanoliter scale. We perform dynamic force spectroscopy (DFS)¹⁹ of the liquid drop in shear mode of AFM, where the drop forms a liquid bridge between the shearing tip and the substrate. The DFS method measures independently and

^a Department of Physics and Astronomy, Institute of Applied Physics, Seoul National University, Gwanak-gu, Seoul 151-747, Korea. Fax: +82-2-886-5786; Tel: +82-2-880-6600; E-mail: whjhe@snu.ac.kr

[†] Electronic Supplementary Information (ESI) available: [details of any supplementary information available should be included here]. See DOI: 10.1039/b000000x/

[‡] Present address: Samsung Electronics, Giheung Campus, Yongin 446-920, Korea

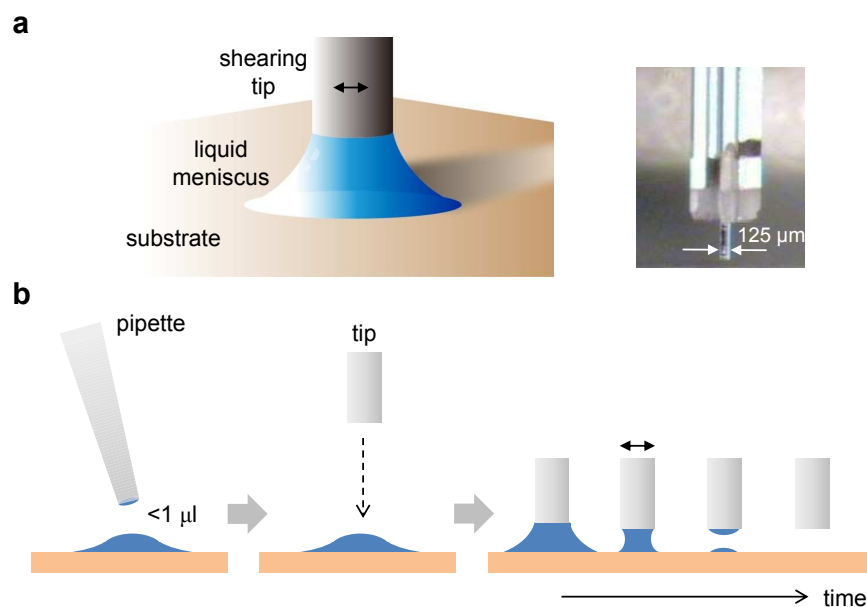


Fig. 1 Experimental schematics and procedures of AFM-based viscometry. **a**, Schematic for viscosity measurement of a sessile droplet using quartz tuning-fork (QTF) based dynamic force spectroscopy of nanoliter water bridge (left). Here the cylindrical probe tip is prepared by attaching the cleaved piece of optical fiber to one prong of the tuning fork, as shown in the photo image (right). **b**, Firstly, we release a minute droplet of liquids ($\ll 1 \mu\text{l}$) on the mica substrate. Secondly, we bring the tip, oscillating at the frequency near resonance for maximum sensitivity, onto the sessile drop until the tip bottom touches gently the liquid. Then, we start recording the amplitude and phase of the tip motion until the bridge is evaporated. Finally, we obtain the resonance curve of tip oscillations at the same tip position to find the reference state with zero interaction.

simultaneously the elastic as well as damping forces induced by the liquid bridge^{20,21}. We observe that the elastic force with negative-valued elasticity results entirely from the hydrodynamic responses of the bulk phase inside the nanoliter liquid bridge, whereas the damping force comes from both bulk and interfacial phases. Therefore, as we shall show later, the liquid viscosity can be obtained from the elastic interaction of the sheared nanoliter liquid bridge, independently of the boundary interfacial effects.

Materials and Methods

We have performed DFS of a sessile drop of water at about 1 nanoliter on mica substrate, by using a home-made, shear-mode, quartz tuning-fork (QTF)-based AFM, as illustrated in Fig. 1a (left panel). The QTF has a high spring constant ($\sim 10^4 \text{ N/m}$) and high quality factor ($\sim 10^3$), and thus sensitive measurements can be made without the jump-to-contact instability, which is a typical limiting factor for precise distance control of liquid bridges in the cantilever-based AFM. A cleaved optical fiber is used as a tip, which has a flat bottom with $125 \mu\text{m}$ diameter and is attached to one prong of QTF (right panel). When this hydrophilic tip touches the sessile drop, the drop spontaneously forms a liquid bridge between the tip and the substrate, and we measure the shear interaction with the bridge quantitatively by DFS method^{22–24}. The DFS represents the tip-sample interaction F_{int} as a sum of the elastic and damping components; $F_{\text{int}} = F_{\text{k}} + F_{\text{b}} = -k_{\text{int}}x - b_{\text{int}}v$, where F_{k} is the elastic force, F_{b} the damping force, k_{int} the elasticity, b_{int} the damping constant, and x (v) is the position (velocity) of the tip. Interestingly, we find that the liquid viscosity is proportional to the square of the negative elasticity.

We have used a cleaved optical fiber tip and a mica substrate for shear-mode operation of AFM by the following steps. We first prepared a piece of optical fiber cleaved by a diamond cutter, and carefully aligned and glued to one prong of QTF (Fig. 1a (right)). We cleaned the side wall and bottom surface of the fiber tip by dipping it in the solution of dilute acid 5% (acetic acid) and then rinsed by deionized water. For the mica substrate, a freshly cleaved mica was rinsed by dilute acid 5% (acetic acid) and then by deionized water. Both the tip and the substrate were dried by blowing nitrogen gas for several minutes until any remaining water on both the tip and substrate surfaces were removed. In addition, we also performed experiments using the gold and HOPG substrates, and obtained consistent results (see Supplementary Fig. S1), which demonstrates that our experimental results are insensitive to the specifics of the used substrates.

The experimental procedures for DFS of the nanoliter water droplet is described in Fig. 1b. We first release a small volume of deionized water ($\ll 1 \mu\text{l}$) on mica substrate using the micropipette, and approach the fiber tip by a motorized positioning system until the tip bottom is gently immersed in the drop. Then, the drop transforms into the bridge and we record the amplitude and phase of the tip oscillation until the bridge is ruptured and evaporated. Finally, the free resonance curve is obtained for *in situ* calibration of zero external interaction.

Results and Discussions

Dynamic force spectroscopy of nanoliter liquid bridge

Figure 2a shows detailed shapes of the sheared water drop during DFS. Here, the tip oscillates at $\omega/2\pi \approx 32 \text{ kHz}$ frequency with $A \approx$

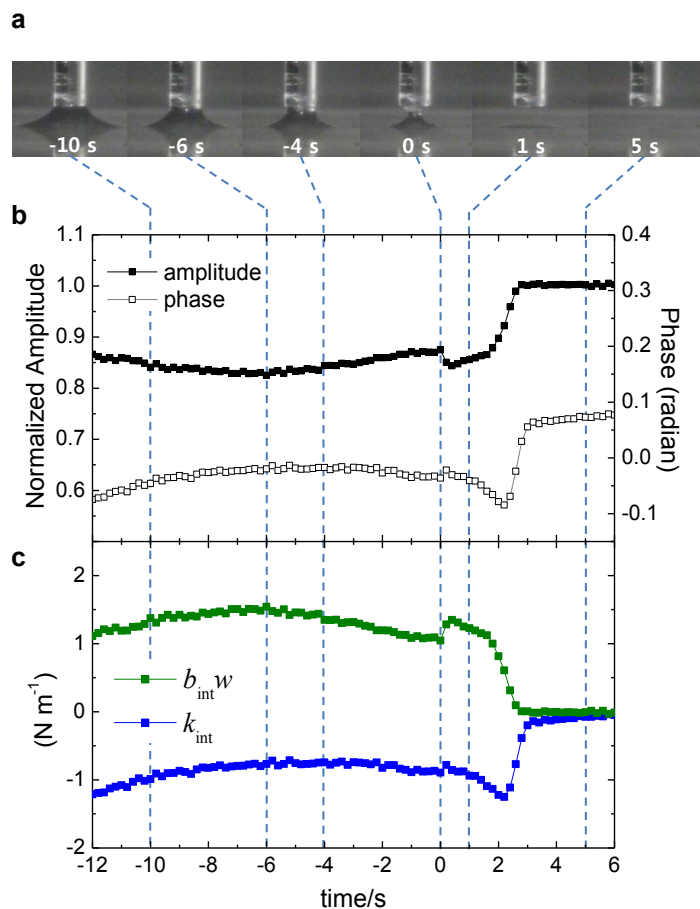


Fig. 2 Dynamic force spectroscopy of a sessile water droplet. **a**, Optical micrographs showing the shapes of the sessile drop during force measurements. The liquid droplet forms a bridge between the hydrophilic tip and the hydrophilic mica substrate ($t = -10$ s), the neck of bridge becomes narrow due to evaporation ($t = -10 \sim -0$ s), the bridge is ruptured (just after $t = 0$), and the remnants remaining on the tip and substrate ($t = 1$ s) evaporate ($t = 5$ s). **b**, Normalized amplitude and phase of the AFM tip measured as a function of time, where the amplitude was normalized by the mean amplitude at zero interaction ($t = 5$ to 7 s). The vertical broken lines indicate the times when the optical images in (a) were taken. **c**, Elastic k_{int} and damping $b_{int} w$ coefficients obtained from the amplitude and phase information by dynamic force spectroscopy^{19,22}.

1 nm amplitude. When the tip touches the boundary surface of a sessile drop, the drop immediately forms into a liquid bridge in the tip-substrate gap. As the liquid bridge evaporates, the liquid-solid contact line on the side wall of the tip slides down ($t = -10$ s) until it reaches the circumference at the flat bottom of tip, where it first sticks ($t = -6$ s), the neck of the bridge then gets narrower ($t = -4$ s), and finally the bridge is ruptured ($t = 0$). Notice that a tiny amount of liquid left on the tip bottom and the mica substrate after the rupture soon evaporates and disappears ($t = +5$ s).

Figures 2b and 2c present the temporal change of the amplitude and phase of the tip oscillation measured during shear of the water bridge, and the associated tip-sample interaction represented by k_{int} and $b_{int} w$, respectively. Although the tip response results from complex interplay between oscillatory drive and fluid dynamics, one can obtain explicitly the tip-sample interaction us-

ing the DFS method. In Fig. 2c, we observe that the shear interaction with the nanoliter liquid is manifested by both the negative elasticity and the positive damping coefficient ($t = -12 \sim 0$ s). While the viscous nature of liquids may describe naturally the observed positive damping, the negative elasticity or the anti-elastic force looks counter-intuitive at first glance.

In general, the ‘negative’ elasticity produces unstable behaviors as shown in novel composite materials²⁵ and hair bundles in ears²⁶. Nonetheless, such an instability does not occur in the present system because the elasticity of the entire system is still positive, as given by the sum of the QTF stiffness ($\approx 27,000$ N/m) and the negative elasticity of sheared liquid (≈ -0.8 N/m). Previously, we observed the positive-valued elasticity for the zeptoliter liquid bridges, resulting from the appreciable surface-energy change at the similar shear displacement of ~ 1 nm²⁰. However, in the case of nanoliter liquid, the surface-energy change is completely negligible under the nanometric shear, and thus positive elasticity is absent. The negative elasticity comes from the retarded response of the fluid, associated with the fluidic inertia^{27,28}. This hydrodynamic memory can induce a force in-phase with respect to the the tip oscillation in the inertial regime, where the height of the bridge should be much larger than the viscous penetration depth²⁷. Indeed, the bridge height is about $100 \mu\text{m}$, whereas the penetration depth is $\delta = \sqrt{2\eta/(w\rho)} \approx 4 \mu\text{m}$ in our case, where η is the viscosity and ρ the liquid density. We also observe the magnitude of elasticity decreases, while showing persistent damping, as the mass (or inertia) of the sheared droplet reduces due to evaporation ($t = -12 \sim 0$ s in Fig. 2) (Supplementary Fig. S2).

Contact area-mediated interaction with nanoliter liquid bridge

For quantitative understanding of the measured k_{int} and $b_{int} w$, we analyze the specific geometry of the bridge described in Fig. 3a, in which the contact line sticks to the circumference of the tip bottom so that the neck of the bridge is same as the tip diameter. This particular bridge shape corresponds to what is formed at $t = -6 \sim -4$ s (Fig. 2a), where the tip-liquid interaction occurs only on the tip bottom-surface, but not on the side wall of the cylindrical tip. In such a state, the liquid bridge-induced force is applied only on the liquid-solid contact area (F_{area}) as well as the liquid-solid-air contact line (F_{line}) at the tip bottom (Fig. 3a), which facilitates unambiguously our theoretical analysis.

For such a well defined bridge configuration, we first derive analytically the contact-area interaction force by constructing a model consisting of two infinite plates as described in Fig. 3b. The upper plate represents the oscillatory driven tip and its motion described by,

$$m\ddot{x} + b\dot{x} + kx = Fe^{i\omega t} + F_{area}, \quad (1)$$

where m is the effective mass of the probe, b the intrinsic damping constant, k the stiffness of the probe, $Fe^{i\omega t}$ the driving force, and F_{area} the liquid-mediated shear force exerted on the contact area (i.e., on the bottom surface of the tip). The contact-area force

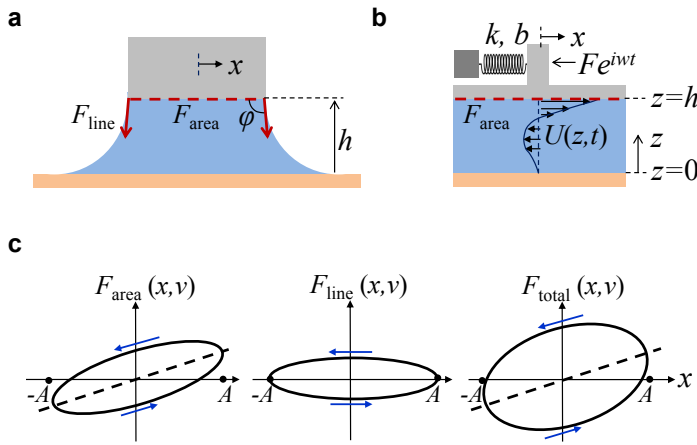


Fig. 3 Theoretical model for the coupled system of AFM tip and confined liquid. **a**, Schematics of the tip shearing the liquid bridge, where the tip interacts with the bridge on the contact area at the tip bottom as well as on the contact line at the circumference of the tip. **b**, For the specific geometry of liquid bridge described in (a), one can derive explicitly the analytical expressions of the contact-area interaction by using a two-dimensional model of confined liquid under oscillatory shear. **c**, Schematics of interaction forces experienced by the tip as a function of the instantaneous tip position during oscillatory shear motion. While the contact-area interaction generates both the elastic and damping forces, the contact-line interaction induces only the additional damping for the nanometric shear motion of the nanoliter-volume liquid bridge (see text for details). The total force is the sum of the contact-area and contact-line forces.

F_{area} is given by the product of the contact area σ and the stress tensor τ_{ij} at the interface,

$$F_{\text{area}} = -\sigma \tau_{xz}(h) = -\sigma \eta \partial U / \partial z|_{z=h}, \quad (2)$$

where U is the velocity field of the fluid in the x -direction and only the xz -component of τ_{ij} is considered due to the two-dimensional symmetry of the system. For an incompressible Newtonian fluid with that symmetry, the Navier-Stokes equation for $U(z,t)$ becomes²⁷,

$$\frac{\partial U}{\partial t} = \frac{\eta}{\rho} \frac{\partial^2 U}{\partial z^2}. \quad (3)$$

Therefore, F_{area} can be obtained by solving the coupled equations (1) to (3) with no-slip boundary condition at the upper and lower interfaces, such that $U(z=h,t) = \dot{x}(h,t)$ and $U(z=0,t) = 0$.

For the present oscillatory system, we look for periodic solutions for both the probe motion $x(h,t)$ and the fluid flow $U(z,t)$ in the forms, $U(z,t) = u(z) e^{i(\omega t + \theta)}$ and $x(h,t) = A e^{i(\omega t + \theta - \pi/2)}$. By substituting these into Eqs. (1) to (3), we obtain,

$$F_{\text{area}} = -(1+i) \cot\{(1-i)h/\delta\} \kappa x, \quad (4)$$

where $\delta = \sqrt{2\eta/(\omega\rho)}$ is the viscous penetration depth and $\kappa = \sigma \omega^{3/2} \sqrt{\eta\rho}/2$. Notice that the real part of F_{area} corresponds to the position (or acceleration) dependent force ($\ddot{x} = -\omega^2 x$) while the imaginary part to the velocity-dependent force ($v = i\omega x$). Thus, F_{area} can be understood as the sum of elastic and damping forces, from which we obtain the force coefficients k_{int}

and b_{int} . Although the coefficients are highly nonlinear functions of the confining height h , they converge to constant values as $h \rightarrow \infty$ ²⁹; $k_{\text{int}} = -b_{\text{int}}\omega = -\kappa$. This indicates that we obtain the negative elasticity in the nanoliter-volume liquid droplet, as observed in experiment (Fig. 2c). Notice that this contact-area interaction predicts equal magnitudes of $|b_{\text{int}}\omega| = |k_{\text{int}}|$, whereas the experiment shows the slightly higher damping, $|b_{\text{int}}\omega| > |k_{\text{int}}|$ (Fig. 2c), as will be discussed below.

Contact line-mediated interaction with nanoliter liquid bridge

Let us demonstrate that the additional damping observed beyond Eq. (4) is attributed to the contact-line interaction. While the Young's law predicts a unique value of contact angle at the three-phase contact line in equilibrium, the contact angle generally varies as the contact line moves^{30,31}. This dynamic contact angle hysteresis depends on the velocity of the contact line relative to the solid surface in contact, and induces a force per unit length, $\gamma \cos \phi$, in the horizontal direction, where γ is the surface tension of water and ϕ is the dynamic contact angle (Fig. 3a). In our oscillatory system, the contact line can move relative to the tip surface when the tip moves. This leads to the tip velocity-dependent contact-line force, F_{line} , given by the summation of the components, $\gamma \cos \phi$, around the contact line²⁰. Therefore, F_{line} produces a tip-velocity dependent dissipative force and is experienced by the tip within one period of oscillation, as schematically drawn in the middle of Fig. 3c. When the tip is at $x = \pm A$, F_{line} becomes zero because $v = \dot{x} = 0$. However, when $x = 0$ (or $v = \pm \omega A$), the force exhibits two different values with the same magnitude but opposite sign depending on the moving direction of the tip. Thus, such a hysteretic force induces energy dissipation, given by the area enclosed by the black curve in Fig. 3c (middle), resulting in the measured extra damping²⁰. In Fig. 3c, the total interaction force versus the instantaneous tip position is presented by the sum (right panel) of the contact-area (left panel) and the contact-line (middle panel) forces. The slope marked by the dashed line represents the negative elasticity, which is not affected by the additional damping due to F_{line} . Notice that this analysis allows to disregard completely the interfacial effects in the viscosity measurement of an extremely minute-volume liquids, which is not achieved by the conventional rheometers.

Here we estimate the contact line-induced additional damping from the hydrodynamics theory³². The viscous flow in the proximity of the moving contact line alters the contact angle as $\phi^3 - \phi_{\text{eq}}^3 \approx 9Ca l$, where ϕ_{eq} is the equilibrium contact angle, Ca the capillary number, and l a logarithmic factor in the range of 1 to 100. For $l \sim 100$, the maximal angle change per unit oscillation amplitude, $(\phi_d - \phi_{\text{eq}})/A$, is about a few 10^{-5} rad/nm, which results in the damping of about 0.5 N/m (Supplementary Note). This gives a reasonable agreement with the measured extra damping presented in Fig. 2c (and inset of Fig. 4c), where $b_{\text{int}}\omega - |k_{\text{int}}| \approx 0.7$ N/m. Notice that we observed previously a logarithmic increase of damping with respect to the shear amplitude for the case of the 'nanometric' liquid bridges, which was well described by the pinning-depinning kinetics of the

contact line in the molecular-kinetic theory³⁰. In the present ‘macroscopic’ bridges, on the other hand, the damping does not depend on the amplitude A (inset of Fig. 4c for sample II), but is fully explained by the hydrodynamic ‘viscous’ damping that occurs on the contact area as well as the contact line.

Determination of the viscosity from negative elasticity in nanoliter liquid bridge

Finally, we derive explicitly the viscosity (η) from the negative elasticity (k_{int}) obtained by DFS. From Eq. (4), we obtain the following formula (Supplementary Note),

$$\eta = 2k_{\text{int}}^2 / (\sigma^2 w^3 \rho). \quad (5)$$

Figure 4 shows the plots obtained by evaluation of Eq. (5), using the elasticity information (Fig. 2c) for four successive experiments. Since the model (Figs. 3a and 3b) and the formula Eq. (5) are valid only for the specific bridge shape available at $t = -6 \sim -4$ s (Fig. 2a), we analyze the data only within this time window in Fig. 4a to determine the viscosity. Figure 4c presents the calculated viscosity (filled black symbols for sample I) showing reasonable agreement with the actual viscosity of water at 29°C (solid line), where the empty black square is the average of four data set.

To justify the validity of our methodology, we have performed similar experiments for the water bridge at milliliter scale (Fig. 4b). Since our model is intrinsically scale-independent, we find consistent results (red symbols) with those for the nanoliter droplets (black), as shown in Fig. 4c. In the milliliter droplet experiments (sample II), we have evaluated Eq. (5) by taking the data at $t = -10 \sim 0$ s (Fig. 4b) to determine the viscosity. Moreover, the inset of Fig. 4c shows that the measured elastic and damping coefficients (sample II) are independent of the shear amplitude, which is the case as long as the amplitude is small enough to induce no change of surface energy and thus to produce zero positive elasticity.

Let us now discuss the temperature effect on the viscosity of nanoliter liquids. Although two independent sets of experiments for nanoliter (sample I) and milliliter (sample II) liquids result in the same values of water viscosity (open black/red symbols in Fig. 4c), the data fluctuations for sample I are slightly higher than for sample II (filled black/red symbols). A possible reason is that the viscosity of nanoliter liquids is more sensitive to the ambient conditions, such as temperature variation, than that of milliliter liquids. In our experiments, since we have illuminated light for video recording to monitor the details of the liquid shapes, the light can increase the temperature of the air, the AFM body and the chamber. In particular, since the AFM body and chamber are made of metallic materials, their temperature and thus the temperature of water bridge can vary easily together. For example, if a light of 10 watt power is absorbed for 100 s by a metal of 100 g mass, the temperature change ΔT is about 20°C. If this temperature change of 20°C occurs in the nanoliter drop of water by 17 ~ 37°C, the viscosity can vary by 0.69 ~ 1.08 m·Pa·s, comparable to the experimentally observed variations (filled

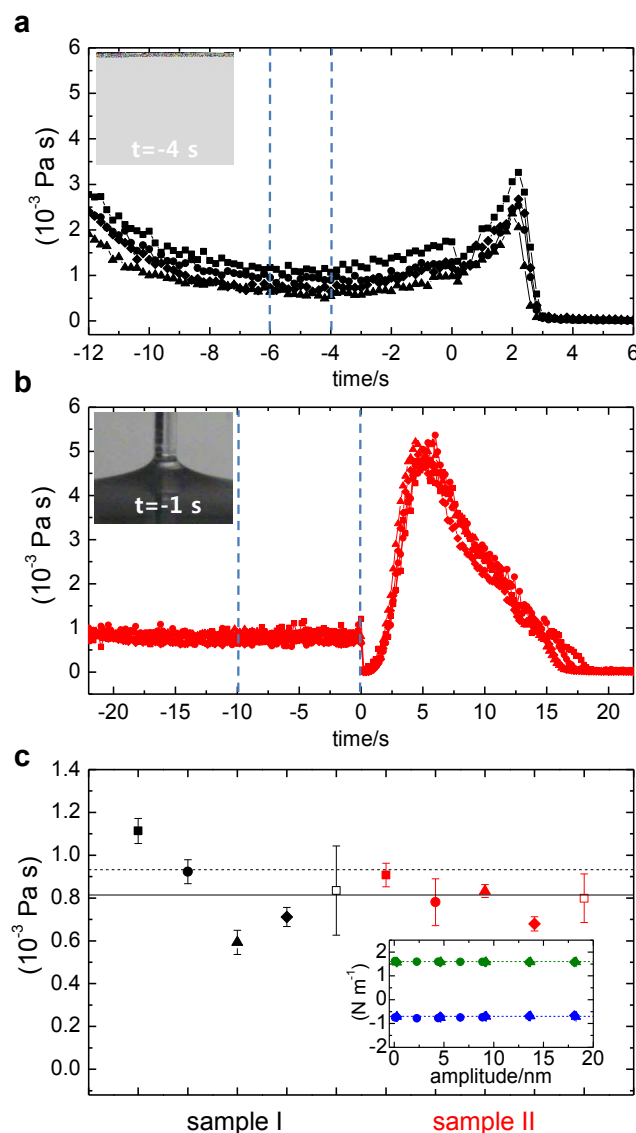


Fig. 4 Determination of viscosity for nanoliter water and comparison with milliliter water. **a**, Derivation of viscosity (Eq. (5)) by using the elasticity information k_{int} for four successive experiments including Fig. 2c. **b**, Results for a much larger water bridge of about 1 ml volume. Here, the shearing height with respect to the bottom is about 3 mm (inset). **c**, Plot of the viscosity values obtained by the data in the range of $t = -6$ to -4 s in Fig. 4a (filled black dots, sample I) and in the range of $t = -10$ to 0 s in Fig. 4b (filled red dots, sample II). The black empty square denotes the average value of viscosity for the nanoliter water, and the red empty square for the milliliter water. The error bars indicate the standard deviations of the data considered in each analysis. During the experiments, the ambient room temperature was about 23°C, at which the viscosity of water is 0.93×10^{-3} Pa s, indicated as dashed line. The solid line represents the viscosity of water at 29°C. Inset: The elastic (blue) and damping (green) coefficients versus the shear amplitude for sample II, obtained at around $t = -20$ s in Fig. 4b, where the dashed lines are the eye guides.

black symbols, Fig. 4c). For the milliliter liquids, the temperature variation could be less than that of nanoliter liquids during the measurement, due to the much larger liquid volume and the associated higher heat capacity. Thus, the smaller temperature variation of viscosity is obtained compared to the nanoliter water, as observed in experiments. Notice that the nonnegligible viscosity variation in the milliliter droplets could be also due to the local temperature fluctuations near the shearing tip and thus use of a temperature-controlled sample stage may further enhance the measurement accuracy.

Conclusions

We have demonstrated an AFM-based platform for the viscosity measurement of liquids at nanoliter scale, and have proved its validity for water, a ubiquitous Newtonian fluid. Despite the high surface-to-volume ratio of nanoliter liquids, we have probed the purely viscous flow-associated resistance, or the viscosity, by measuring the negative elasticity that originates from the hydrodynamic memory effects²⁸. To extend the present technique to the non-Newtonian fluids, one should develop theoretical tools that deal with the coupled motion of the AFM probe and the non-Newtonian fluids. In addition, to investigate the frequency dependence of the measured quantities, a probe with variable resonance frequency is also needed. Furthermore, by employing a nano-apertured pipette³³ to dispense and measure the 'net' sub-nanoliter liquid, we can reduce our unrecoverable volume of 1 nanoliter, at least by a factor of 100 with a smaller fiber tip. We are currently developing the theoretical method and experimental platform for versatile realization of the AFM-based sub nanoliter-scale rheometry useful for nano-biological and medical applications^{1,2}.

Acknowledgements

This work was supported in part by the National Research Foundation of Korea (NRF) grant funded by the Korea government (MSIP) (No. 2011-0029541.)

Notes and references

- 1 G. Lowe, A. Rumley, J. Norrie, I. Ford, J. Shepherd, S. Cobbe, P. Macfarlane, C. Packard, Blood rheology, cardiovascular risk factors, and cardiovascular disease: the West of Scotland Coronary Prevention Study. *Thromb Haemost.* 84, 553-558 (2000).
- 2 M. Thibaud, Z. Shen, J. Harting, C. Misbah, Prediction of anomalous blood viscosity in confined shear flow. *Phys. Rev. Lett.* 112, 238304 (2014).
- 3 E. W. Merrill, Rheology of Blood, *Physiological Reviews* 49, 863-888 (1969).
- 4 M. A. Gertz, R. Fonseca, S. V. Rajkumar, Waldenström's Macroglobulinemia, *The Oncologist* 5, 63-67 (2000).
- 5 N. Srivastava, R. Davenport, M. Burns, Nanoliter viscometer for analyzing blood plasma and other liquid samples. *Anal. Chem.* 77, 383-392 (2005).
- 6 N. Srivastava, M. Burns, Analysis of non-Newtonian liquids using a microfluidic capillary viscometer. *Anal. Chem.* 78, 1690-1696 (2006).
- 7 E. Livak-Dahl, J. Lee, M. Burns, Nanoliter droplet viscometer with additive-free operation. *Lab Chip* 13, 297-301 (2013).
- 8 P. Rust, D. Cereghetti, J. Duala, A micro-liter viscosity and density sensor for the rheological characterization of DNA solutions in the kilo-hertz range. *Lab Chip* 13, 4794-4799 (2013).
- 9 S. Keen, *et al.*, Multipoint viscosity measurements in microfluidic channels using optical tweezers. *Lab Chip* 9, 2059-2062 (2009).
- 10 G. Christopher, J. Yoo, N. Dagalakis, S. Hudson, K. Migler, Development of a MEMS based dynamic rheometer. *Lab Chip*, 10, 2749-2757 (2010).
- 11 K. Eom, H. S. Park, D. S. Yoon, T. Kwon, Nanomechanical resonators and their applications in biological/chemical detection: nanomechanics principles. *Phys. Rep.* 503, 115-163 (2011).
- 12 J. W. Beams, D. W. Kupke, Simultaneous measurements of viscosity and density in solutions undergoing change. *Proc. Natl. Acad. Sci. USA* 74, 4430-4433 (1977).
- 13 T. Mason, D. Weitz, Optical measurements of frequency-dependent linear viscoelastic moduli of complex fluids. *Phys. Rev. Lett.* 74, 1250 (1995).
- 14 T. G. Mason, K. Ganesan, J. H. Zanten, D. Wirtz, S. C. Kuo, Particle tracking microrheology of complex fluids. *Phys. Rev. Lett.* 79, 3282 (1997).
- 15 J. Crocker, M. Valentine, E. Weeks, T. Gisler, P. Kaplan, A. Yodh, D. Weitz, Two-point microrheology of inhomogeneous soft materials. *Phys. Rev. Lett.* 85, 888 (2000).
- 16 J. E. Sader, Frequency response of cantilever beams immersed in viscous fluids with applications to the atomic force microscope. *J. Appl. Phys.* 84, 64-76 (1998).
- 17 M. Papi, *et al.*, Detection of microviscosity by using uncalibrated atomic force microscopy cantilevers. *Appl. Phys. Lett.* 93, 124102 (2008).
- 18 E. Gil-Santos, *et al.*, High-frequency nano-optomechanical disk resonators in liquids. *Nature Nanotech.* 10, 810-816 (2015).
- 19 R. García, R. Pérez, Dynamic atomic force microscopy method. *Surf. Sci. Rep.* 47, 197-301 (2002).
- 20 M. Lee, B. Kim, J. Kim, W. Jhe, Noncontact Friction via Capillary Shear Interaction at Nanoscale. *Nat. Commun.* 6, 7359 (2015).
- 21 B. Kim, S. Kwon, M. Lee, Q. Kim, S. An, W. Jhe, Probing nonlinear rheology layer-by-layer in interfacial hydration water. *Proc. Natl. Acad. Sci. USA* 112, 15619-15623 (2015).
- 22 M. Lee, W. Jhe, General theory of amplitude-modulation atomic force microscopy. *Phys. Rev. Lett.* 97, 036104 (2006).
- 23 M. Lee, J. Jahng, K. Kim, W. Jhe, Quantitative atomic force measurement with a quartz tuning fork. *Appl. Phys. Lett.* 91, 023117 (2007).
- 24 M. Lee, B. Sung, N. Hashemi, W. Jhe, Study of a nanoscale

- water cluster by atomic force microscopy. *Faraday Disc.* 141, 415-421 (2009).
- 25 R. S. Lakes, T. Lee, A. Bersie, Y. C. Wang, Extreme damping in composite materials with negative-stiffness inclusions. *Nature* 410, 565-567 (2001).
- 26 L. L. Goff, D. Bozovic, A. J. Hudspeth, Adaptive shift in the domain of negative stiffness during spontaneous oscillation by hair bundles from the internal ear. *Proc. Natl. Acad. Sci. USA* 102 16996-17001 (2005).
- 27 D. L. Landau, E. M. Lifshitz, *Fluid Mechanics* (Pergamon Press, Third Revised English Edition, 1966).
- 28 T. Franosch, *et al.*, Resonances arising from hydrodynamic memory in Brownian motion. *Nature* 478, 85-88 (2011).
- 29 Here we use the approximation, $\cot((1-i)x) \approx i$ if $x \gg 1$.
- 30 T. D. Blake, J. M. Haynes, Kinetics of liquid/liquid displacement. *J. Colloid. Interface Sci.* 30, 421-423 (1969).
- 31 J. N. Israelachvili, *Intermolecular and Surface Forces* (Academic Press, London, 2003).
- 32 R. G. Cox, The dynamics of the spreading of liquids on a solid surface. *J. Fluid Mech.* 168, 169-194 (1986).
- 33 S. An, C. Stambaugh, G. Kim, M. Lee, Y. Kim, K. Lee, W. Jhe, Low-volume liquid delivery and nanolithography using a nanopipette combined with a quartz tuning fork-atomic force microscope. *Nanoscale*, 4, 6493-6500 (2012).